Aust. J. Phys., 1980, **33**, 549–59

A Two-accelerator Facility and Its Use for Radiation Damage Studies in Alkali Halides

C. S. Newton and H. J. Hay

Department of Nuclear Physics, Research School of Physical Sciences,
Australian National University, P.O. Box 4, Canberra, A.C.T. 2600.

Abstract

An experimental system is described in which heavy ions of energies 50–100 MeV, and light ions of energies 0·5–2 MeV, may be transported alternatively from different accelerators into a common scattering chamber. Details are given of the beam transport and scattering chamber, the latter being designed to make in-beam studies of different modes of radiation damage in the target material. An on-line experimental control and data acquisition system with an IBM 1800 computer is used. Experimental studies are described of simultaneous detection of backscattered helium ions, X-rays and optical absorption in single-crystal alkali halide samples, performed during continuous irradiation by a 1 MeV helium beam, as well as of backscattered protons following intermittent irradiation by a 60 MeV oxygen beam. Analysis of the relative damage by these two beams is discussed in relation to a damage mechanism due to Pooley.

1. Introduction

In previous studies of helium-ion induced radiation damage in single crystals (Newton *et al.* 1976), it has been shown that channeling, characteristic X-ray production and optical absorption provide useful information on some details of the damage mechanism. It was shown that the observed backscattering of a beam aligned to a crystal axis provides a powerful method of interpreting the dechanneling due to radiation damage. In order to extend this work to the study of heavy-ion induced damage, beams from the A.N.U. 14 UD Pelletron accelerator were used in the layout shown in Fig. 1. In this arrangement, separate beams from the 14 UD and from a 2 MV Van de Graaff accelerator may be successively switched to the scattering chamber (rather than move the bulky equipment between accelerators). It was found, however, that for a 60 MeV ^{16}O beam bombarding NaCl, no backscattering may be detected, as the yield for such ions above the Coulomb barrier comprises essentially reaction products only. The layout of Fig. 1 obviously permitted alternate ^{16}O and proton irradiations, the latter for backscattering *analysis*: such a procedure almost retains the advantages of an 'in-beam' experiment.

The main requirement to be met by the accelerators was to deliver particle beams with small angular spread ($\lesssim 0{\cdot}01°$) accurately positioned to a common area of a target, with the beam being continuously monitored. These details are described in Section 2*a* below. In Section 2*b* the scattering chamber with provision for recording the three physical effects (backscattering, X-rays and optical absorption) is described. Measurement of beam intensity is described in Section 2*c*, and the detecting equipment in Section 2*d*. A basic need in these experiments was for an efficient data collection

system. This was achieved by a general-purpose data acquisition program, described in Section 3.

Experiments on damage done with this equipment using ^{4}He and ^{16}O beams are illustrated by irradiation studies of NaCl. All the ^{4}He work is described in Section 4. Heavy-ion damage with proton backscattering analysis is described in Section 5*a*, and the results of both irradiations are discussed in Section 5*b* in relation to a theoretical model (Pooley 1966*a*, 1966*b*) for the damage mechanism.

2. Experimental Facilities

(*a*) *Beam Transport*

Fig. 1 shows the two-accelerator beam transport system, with the beam line from the 90° magnet to the target chamber common for both accelerators. This contains the slits S3, quadrupole Q2 and collimator chamber CC, which were aligned to the accelerators by an optical telescope. A laser beam aligned to the same axis was used for setting up items in the target chamber. The layout was similar to that in work described by Price *et al.* (1973).

The common beam line was constructed of stainless steel with metal gaskets, and the system was pumped by a Pfeiffer TCP-400 turbo-molecular pump (at the scattering chamber) and AEI 300 l. s^{-1} triode ion pumps further upstream from the target area.

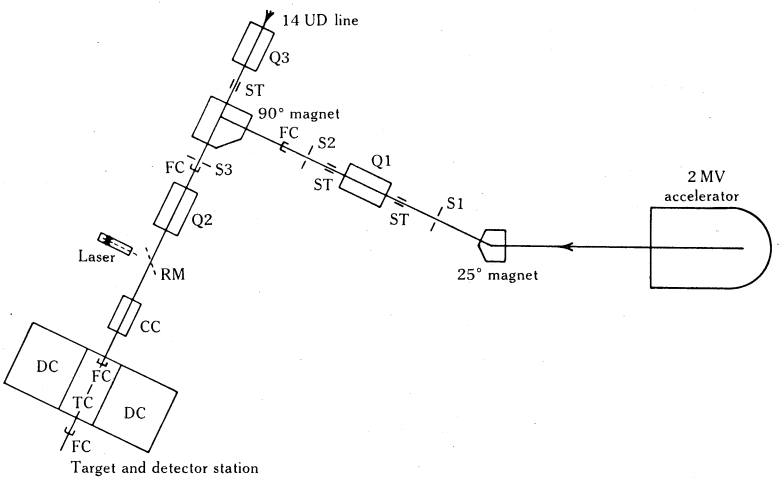

Fig. 1. Layout of the two-accelerator facility for irradiating targets at a common scattering chamber. Elements essential for accurate beam handling and positioning are represented diagrammatically, not to scale: S1, S2 and S3 are beam stabilizing slits; Q1, Q2 and Q3 quadrupole lenses; ST, horizontal and vertical steerers; FC, Faraday cups; CC, collimators and chopper; DC, detector carriage; RM, retractable mirror; TC, target chamber.

(*b*) *Target Chamber*

The stainless steel target chamber was designed and constructed with removable fully-adjustable 'optical bench' bases, with provision for mounting on them previously prepared experimental assemblies. Equipment for which alignment was less critical was mounted on interchangeable lids, and generous provision was made for ports at both sides to accommodate independently adjustable external detectors.

The chamber is rectangular in shape, being 82·5 cm along the beam, 27·5 cm wide and 47·5 cm deep. Copper gaskets provide the permanent vacuum seals, and 'Viton' rubber O-rings are used for ports and for the lid. With the pumping system used, a clean high vacuum of 2×10^{-7} torr ($\equiv3\times10^{-5}$ Pa) is obtained in the empty chamber. With a typical load of target, flexible cables and electric stepping motors, typically $(1–5)\times10^{-6}$ torr may be achieved after a few hours.

The chamber is supported on a framework which also supports a carriage table at each side, for mounting optical monochromators or other large detecting systems. Each carriage is mounted on ball bearings and may be translated horizontally both parallel and at right angles to the beam axis, and also rotated about a vertical axis.

(*c*) *Beam Measurement*

With thin targets, the beam intensity can be measured after transmission at a Faraday cup at the end of the chamber. However, with insulating or thick targets, this is obviously impossible. It was found impracticable to isolate the whole chamber as a Faraday cup. A beam-monitoring system was constructed similar to that described by Hollis (1972). This comprises a gold-plated aluminium 'chopper' with six vanes upstream of the target, facing a surface-barrier detector. The chopper is driven by a 12 position stepper motor (Calderon C 105) and gives a 50% duty cycle; it may be calibrated by using a retractable Faraday cup before the target. The surface-barrier detector monitors particles scattered at 135° to the incident beam by the gold, in a thin layer of thickness 300–3000 Å (30–300 nm), chosen so as to permit good statistical accuracy for the pulse counting. Energy discrimination and pulse pileup in the amplifier were improved by evaporating a layer of carbon between the gold and aluminium, and using absorbing foils before the detector.

Use of the chopper to monitor the amount of beam at the target, about 1 m downstream, meant that there could be no limiting aperture between chopper and target. For this reason the chopper was placed in the centre of the collimator box (CC in Fig. 1) which could provide both beam-defining and antiscatter baffles. With a requirement of a highly parallel beam, e.g. for channeling, it was found desirable also to define the beam at the slits S3, some 4 m upstream, and not to use the quadrupole Q2. Doing this did not affect the chopper's accuracy in any way.

(*d*) *Experimental Detectors for Channeling and Damage Studies*

The sub-assembly for channeling and in-beam optical absorption studies (Newton *et al.* 1976) was mounted on the target-chamber base. The target support was built into a McLean 3-axis goniometer with stepping motors providing angular increments of 0·01°. The essential observation of *channeling* was made by detecting particles backscattered at 135° from a crystal aligned to the beam axis (i.e. χ_{min}). For studies of *radiation damage* in alkali halides, observations of optical absorption and characteristic X-ray emission were also required. These were made with the detectors described further below. A tungsten filament, attached to the goniometer about 2 cm below the target, was placed so as to illuminate the target indirectly, and thereby allow any charge accumulated to be neutralized by electrons (whose current intensity could be monitored at the filament). This eliminated a buildup of potential at the insulating target, which tends to induce background bremsstrahlung from the target in the observed region of the X-ray spectrum and shifts in the backscattered particle spectrum. In addition to this, the target support incorporated a cooling coil, heater

and thermocouple, allowing target temperatures to be maintained between 100 and 800 K.

In-beam observation of optical absorption was made using the system shown in Fig. 2. Light from the quartz iodide lamp entered the chamber through a quartz window and was split by a 'half-silvered' 45° mirror into a transmitted beam, monitored by a monochromator (Heath EUE 700), and a reflected beam. The latter passed through the target and was then reflected at 45° out to a second monochromator (McPherson 218). As shown in the figure, the second 45° mirror was constructed so as to allow passage of the accelerator beam through a 5 mm hole. Light from the monochromators was detected by cooled photomultipliers (EMI 6256 S) operated in pulse-counting mode (Carriveau 1970).

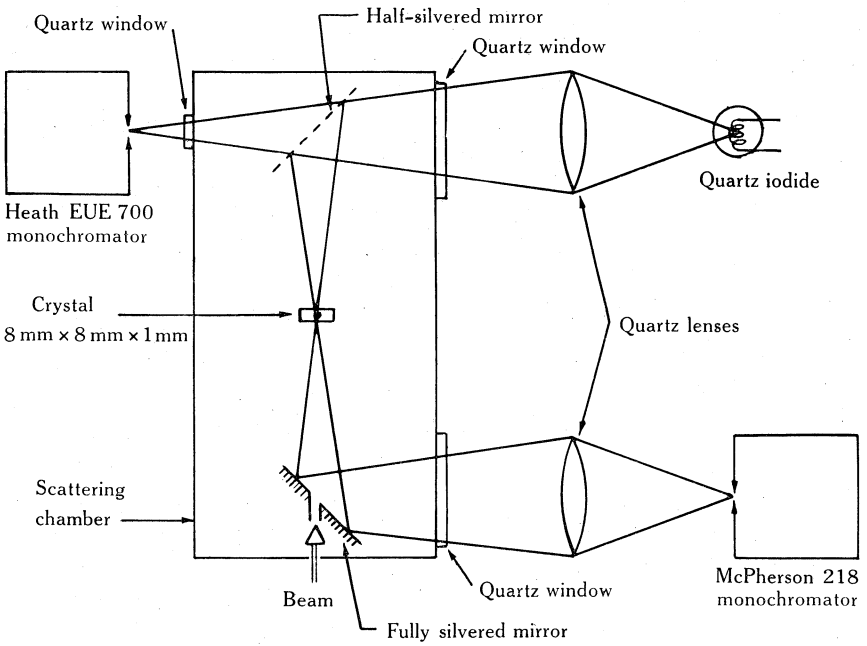

Fig. 2. Schematic view of the light paths in the system for studying optical absorption. The Heath monochromator monitors output from the quartz iodide lamp, and absorption is detected by the McPherson monochromator.

The X-rays were detected in a Si(Li) crystal mounted on the chamber lid at 135° to the beam. A Kevex Model 3050 AA was used of active area 10 mm^2 and thickness 2 mm, incorporating a 2002 A optical feedback preamplifier and a 4510 P main amplifier with pileup rejection capability. Absorbers adequate to stop the scattered beam, and filters to optimize the observed spectral density were mounted in the vacuum on an externally operated wheel. The X-ray detection system was of high resolution, having a capability of 153 eV energy resolution at 5·9 keV; the theoretically available limit is in the region 113–128 eV (Woldseth 1973).

3. Data Recording and On-line Computer Control

Output pulses from detectors and other devices may be recorded in one of several ways. Usually one records a pulse-height spectrum, but it is also useful sometimes to

record data in a 'multiscaled' mode, i.e. a sequence of counts from a single output as a function of an independent variable, such as time. By using a common channel-advance signal, several multiscaled spectra may be recorded simultaneously for subsequent comparison. The same signal may at the same time be used for on-line control of equipment such as a goniometer stepping motor, and thus provide a powerful method of automatic recording of data for a range of external conditions, such as accumulated beam charge, goniometer angle, or indeed any variable of interest. With 3 analogue-to-digital converters (ADC) up to 3 pulse-height spectra (for radiation detectors) and 12 multiscaled spectra (for optical detectors and various beam monitors) were available. The on-line control was needed for crystal alignment as described in Section 4*b* below. The data were recorded using Nuclear Data series 2200 ADCs and locally made computer-controlled scalers, and were stored in the memory of an IBM 1800 computer by a program which also organized the sequence of data flow and changes in externally controlled equipment. Apart from the obvious advantage of speed and convenience, such a program also facilitates rapid sampling and monitor surveillance during data accumulation for identification of any undesired instability or irregularity. The net result is a set of data superior in quantity and quality to that obtained by conventional recording methods.

4. Study of Radiation Damage in NaCl

(*a*) *Objectives of Damage Studies*

It had been found previously (Hollis *et al.* 1973) that, under bombardment by 1 MeV He^+ ions, the aligned backscattering ratio χ_{min} in NaCl appears to increase up to a dose of 10^{15}–10^{16} α particles per cm^2 and decrease thereafter. The present studies were aimed towards understanding the mechanism of this apparent recovery from damage, by simultaneous observation of the three effects already mentioned in Section 2*d*. Whereas an increase of aligned backscattering is a fairly obvious indicator of damage, a measurement of the Na and Cl characteristic X-rays was planned to look for any stoichiometric changes near the surface of the crystal. Also, the optical absorption in the region of the *F*-centre band was chosen as an independent measure of the density of point defects in the region irradiated by the beam.

(*b*) *Crystal Preparation and Alignment*

The NaCl crystals were prepared immediately before mounting in the vacuum system by cleaving along {100} planes into pieces about 1 cm square by 1 mm deep. It was necessary to align the crystal after mounting. Obviously, this can be done by studying channeling about the desired ⟨100⟩ axis, though to do so initially would itself induce damage. Consequently, initial alignment was done by reflecting a He–Ne laser beam from the cleaved surface. The accuracy of this was checked for several crystals by observation of the channeling dip later in the irradiation; the alignment was found to be repeatable to within 0·1°, except when the crystal was so imperfectly cleaved as not to display clear optical reflection. For beam alignment, a modification of the method by Anderson *et al.* (1965) was used: computer-controlled scans with detection of backscattered particles were made in four directions parallel to the sides of a square cone of fairly small included angle ($\lesssim 10°$) surrounding the approximately determined ⟨100⟩ crystal axis. Examination of the planar channeling dips permitted the angular coordinates of the ⟨100⟩ axis to be determined.

(c) Irradiation Runs

After the chopper monitor had been calibrated (Section 2*c*) and the crystal cleaved, mounted and aligned (Section 4*b*), a measurement was made of the optical absorption of the crystal over the wavelength region near the *F*-centre band. The monochromators were then set to the expected peak of the band near 4700 Å (Ivey 1947).

The irradiation was commenced and records were made simultaneously, for a preset time, of two pulse-height spectra (the backscattered particles and the X-rays) and six 400 channel multiscaled spectra, representing the separate Cl and Na characteristic K X-rays, the backscattered particles from just below the surface, the beam monitor (chopper) and the light recorded in both the monitor and absorbed-spectrum monochromators. From a sequence of such records the progress of radiation damage in the crystal was studied as a function of the accumulated dose in beam particles per cm^2. Fig. 3 shows one typical set of records for irradiation of NaCl with a 1 MeV He^+ dose increment of $1{\cdot}5\times10^{12}$ ions cm^{-2}. As the dose increased the damage rate decreased, so the sampling time was lengthened. Records like those in Fig. 3 were taken as 1, 2 or 4 min samples within the total irradiation time which lasted up to 5 days.

Given the data, comprising up to 200 records such as Fig. 3, one was able to plot the progress of the three damage phenomena, each normalized to the irradiating beam. Thus one was able to show how the backscattering ratio varied with dose at each part of the spectrum (Fig. 3*a*) and therefore, knowing the energy loss–depth characteristic (Northcliffe and Schilling 1970), how it varied with *depth* of backscattering. The Na and Cl X-rays were recorded in total (Fig. 3*b*) and separately (Figs 3*c* and 3*d*), and likewise the optical absorption (Figs 3*g* and 3*h*). Subsequent to (non-massive) irradiation, the optical absorption density was of the form given in

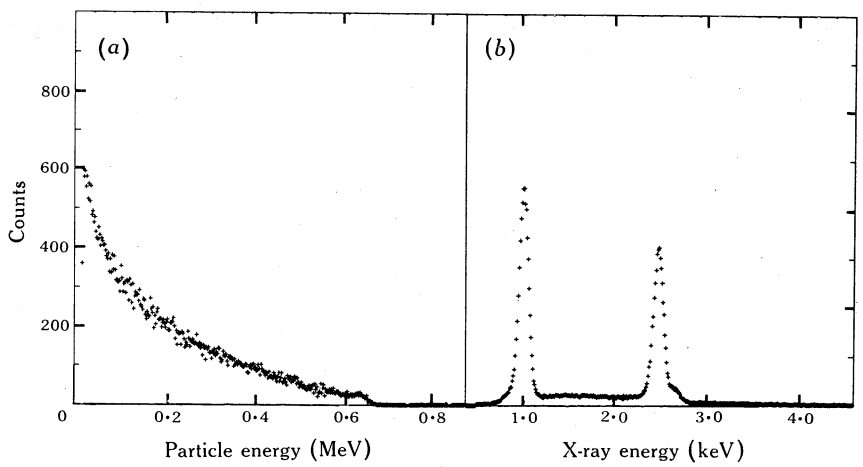

Fig. 3. Records of data simultaneously collected during 4 min irradiation of a NaCl crystal with 1 MeV He ions: (*a*) and (*b*) are energy spectra for total backscattered particles and total X-rays respectively. In (*c*)–(*h*), the multiscaled spectra taken during the irradiation time are shown for the following phenomena: (*c*) Cl X-rays, (*d*) Na X-rays, (*e*) backscattered particles, (*f*) beam monitor, (*g*) light monitor and (*h*) transmitted light. The 135° backscattered particle spectrum in (*a*) shows a surface peak at 0·66 MeV, while the X-ray spectrum in (*b*) shows Na and Cl K_α peaks at 1·041 and 2·622 keV. This record was taken at a total dose of 2×10^{16} cm^{-2}, with a dose increment of $1{\cdot}5\times10^{12}$ cm^{-2}.

Fig. 4, confirming that the monochromators were indeed set at the peak of the absorption band. Typical results of the measurements are shown in Fig. 5*a*, which displays room-temperature data for backscattering from a depth of 1 μm, the Cl X-ray intensity, and optical absorption; all with dose plotted logarithmically from 10^{11} to 2×10^{17} ions cm^{-2}. Reference to Fig. 5*a* shows some interesting variations to be discussed in Section 5. We note here, however, that a practical limit of dose was

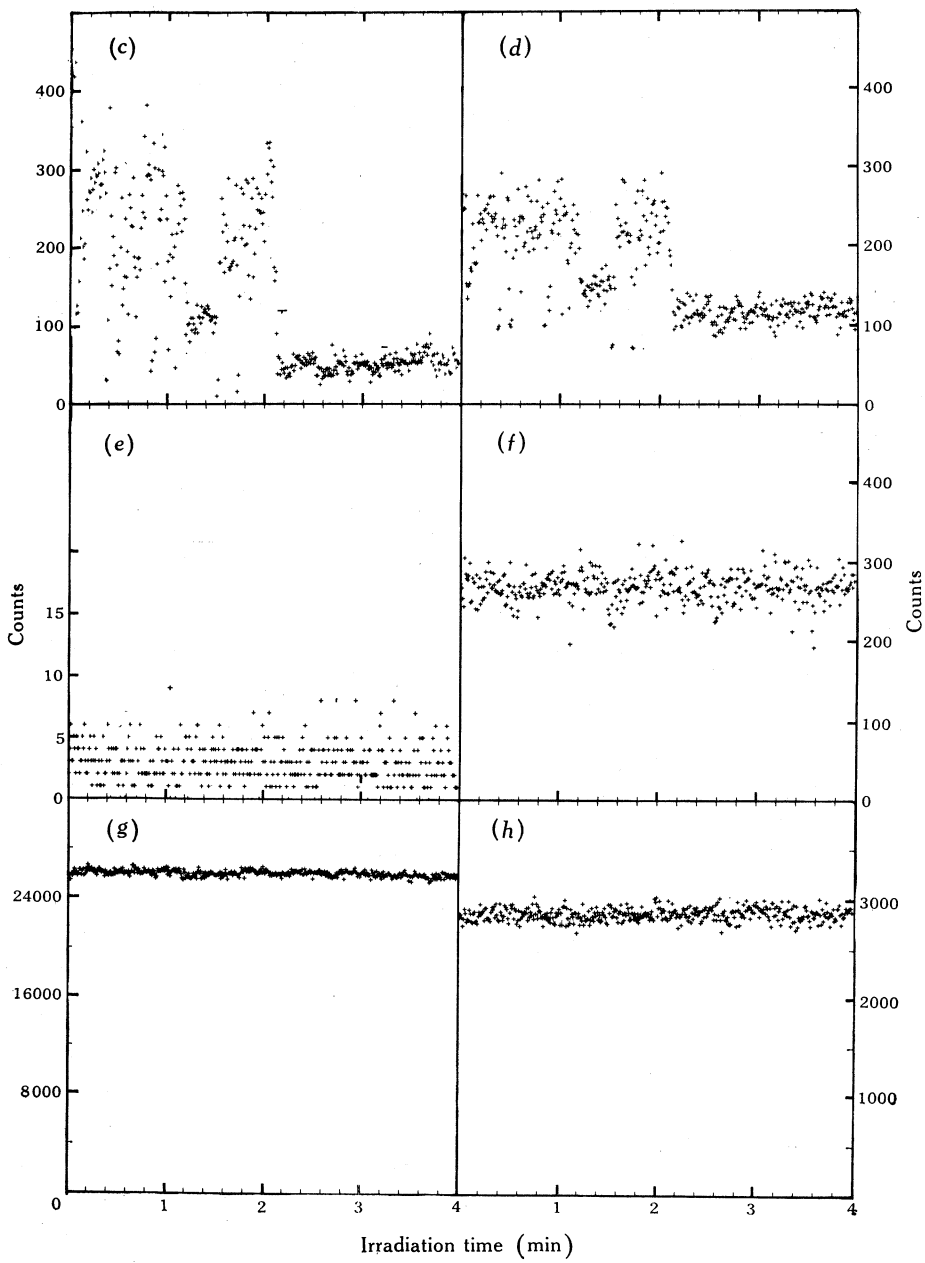

Figs 3*c*–3*h*

reached towards the upper value plotted, as adduced by apparent enormous (and unrepeatable) fluctuations suddenly occurring in the yields from all three crystal-related quantities. Examination under a microscope showed this could be attributed to shattering of the crystal due to weakness induced by massive damage.

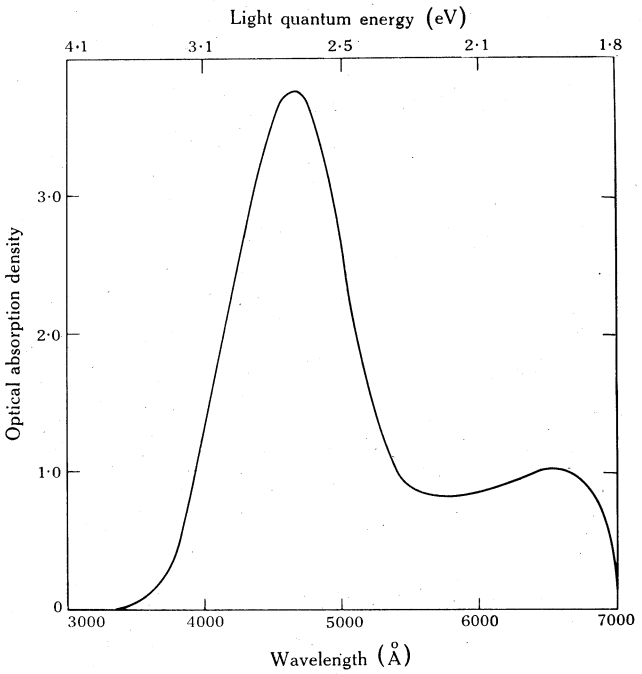

Fig. 4. Optical absorption density of a NaCl crystal damaged by He ions of dose 2×10^{17} cm^2. This curve is obtained from monochromator scans as described in the text. The main absorption peak appears near 4600 Å or 2·7 eV.

5. Comparison of Light and Heavy Ion Damage

(*a*) *Damage by* ^{16}O *Beams*

As discussed in Section 1, it was found feasible to irradiate alkali halide specimens with ^{16}O beams from the 14 UD accelerator and to analyse the damage by backscattering of proton beams. In this work, a study of backscattering alone was undertaken. As will be seen from the discussion in earlier work (Newton *et al.* 1976), this provides the most ready understanding of the damage mechanism. One possible source of difference between the damage due to ^{4}He and ^{16}O beams lies in the well-known distinction of energy loss processes between electronic and nuclear phenomena (Lindhard *et al.* 1963). Whereas the former depends essentially on the incident beam charge and velocity as Z^2/V^2, the latter, being a momentum-recoil effect, is of less importance for the lighter ion. The relative *electronic* stopping powers of 60 MeV ^{16}O and 1 MeV ^{4}He are in the ratio 3·3 to 1 (Northcliffe and Schilling 1970).

Irradiations were made of NaCl by $^{16}O^{5+}$ beams at 60 MeV, the dose being recorded by observation of the chopper backscattering from gold. Between irradiations by chosen increments of dose, backscattering of 1 MeV protons was observed. Care

was taken to use a proton beam *wholly within* the area already irradiated, and also the proton dose was kept at negligible levels. Apart from this, the method of collecting data did not differ from that described in Section 4. The experimental results are shown in Fig. 5*b*, where the backscattering ratio is plotted to correspond to a depth range of 0·8–1·2 μm. The progress of damage shows a rise to maximum at about the same dose as for He ions, however its initial rise is more rapid. Because of the low intensity ^{16}O beam used (chosen to give target heating similar to that of the He beam), doses as high as those seen in Fig. 5*a* were not possible in the limited time available.

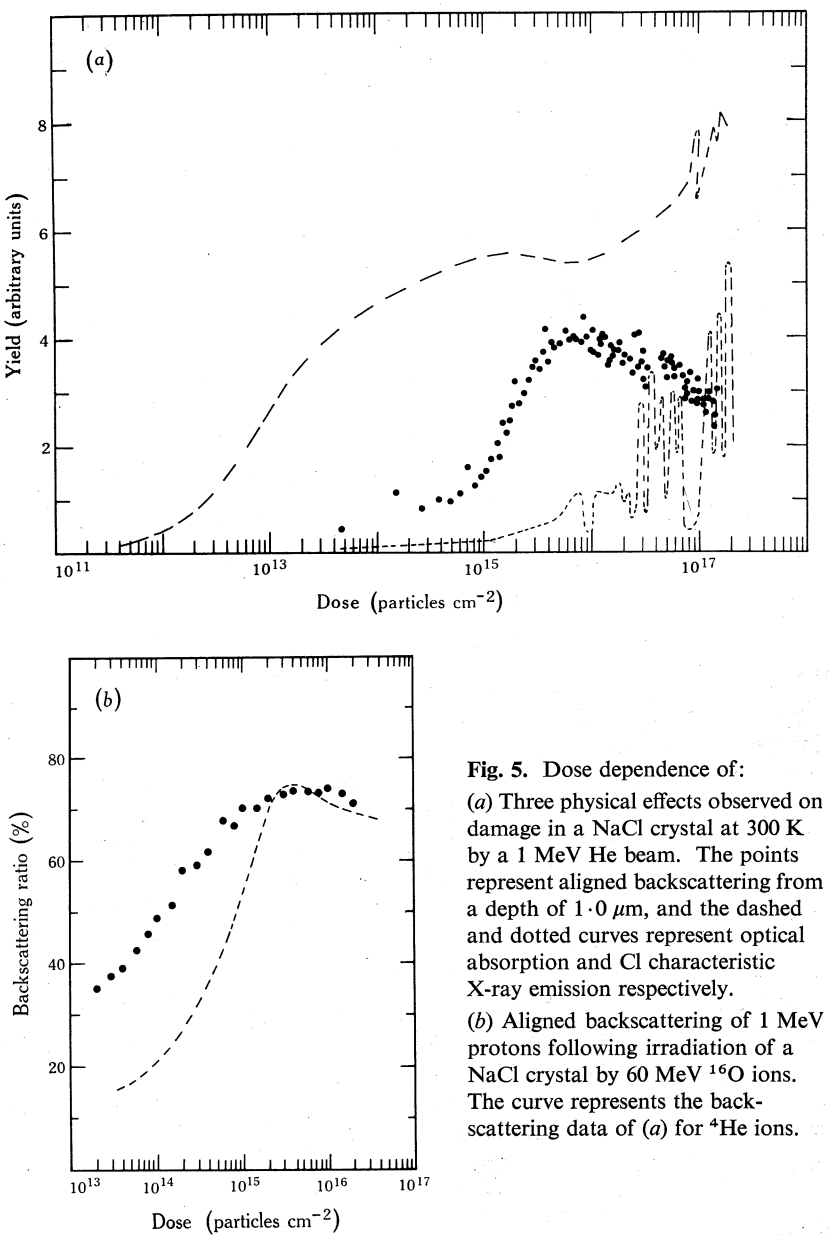

Fig. 5. Dose dependence of:
(*a*) Three physical effects observed on damage in a NaCl crystal at 300 K by a 1 MeV He beam. The points represent aligned backscattering from a depth of 1·0 μm, and the dashed and dotted curves represent optical absorption and Cl characteristic X-ray emission respectively.
(*b*) Aligned backscattering of 1 MeV protons following irradiation of a NaCl crystal by 60 MeV ^{16}O ions. The curve represents the backscattering data of (*a*) for ^{4}He ions.

(b) Comparison of ^{4}He *and* ^{16}O *Damage Mechanisms*

A discussion of the mechanism of damage by 1 MeV ^{4}He ions, as displayed in Fig. 5*a*, has been given by Newton *et al.* (1976). It is of interest here to attempt to relate that mechanism to the observed damage in the same (NaCl) crystal with 60 MeV ^{16}O ions.

Referring to Fig. 5*a*, we see that the optical absorption for He ions appears to rise and saturate at a dose around 10^{15} particles per cm^2. This behaviour is consistent with the 'Pooley' mechanism (Pooley 1966*a*, 1966*b*) in which, with certain alkali halides including NaCl, there is an efficient cooperative mechanism of *F*-centre production which dominates over that due to direct atomic displacement, and the rate is limited by recombination at high *F*-centre density. The backscattering ratio likewise increases with dose, as may be expected due to imperfect channeling following the production of interstitial ions. The Cl X-ray intensity behaves similarly. At a dose near 10^{16} cm^{-2}, all three processes change. The backscattering *decreases*: this has been attributed (Newton *et al.* 1976) to agglomeration of point defects to form linked clusters with ⟨100⟩ axial symmetry, a mechanism observed earlier by Hobbs *et al.* (1972, 1973) in electron microscope studies. The Cl X-ray intensity also decreases, but begins to progressively fluctuate, whereas the optical absorption rises, as shown in Figs 3*c* and 3*d*. (It is noteworthy that the optical absorption shown in Figs 3*g* and 3*h* does not vary.) Although the behaviour of these two phenomena is not understood, it is likely that the effects are due to cracking and increased opaqueness of the crystal near its surface at these large doses.

Considering again the backscattering, which is plotted in Figs 5*a* and 5*b* for effective beam depths 1 μm below the surface, the data show an initial relative *rate* of damage increase by ^{16}O and ^{4}He in the ratio 3 : 1. Beyond a dose of 2×10^{14} cm^{-2} this ratio decreases and at around 6×10^{14} cm^{-2} it falls below unity. These results might be considered surprising, as the initial damage rates come out near the ratio of *electronic* energy losses of 3·3 : 1, which implies that the heavier ion, when channeled, does not impart a significantly greater energy to the lattice atoms than the light one. That this is so may be readily seen as follows. One can show that a 60 MeV ^{16}O ion and a 1 MeV ^{4}He ion, each near its maximum channeling angle ψ_1 (Lindhard 1965), have transverse energies 1200 and 300 eV respectively; they impart a recoil energy E_r to the lattice of 2·9 and 0·7 eV respectively each half-cycle of the channeling trajectory. But the mean energy per lattice atom from each is only of order $E_r\psi_1$, or 0·013 eV in each case. These are both below the 5 eV necessary to create vacancies by the Pooley mechanism, and well below the 30 eV needed for atomic displacement. Hence, in neither case should there be any substantial contribution from recoil effects. In this circumstance, damage is dominated by electronic energy losses, which lead directly to the Pooley process. This process is 'chemical' in that it depends on the motions of valence electrons. The decrease of the relative damage rates below the 3 : 1 ratio is to be expected for larger doses for which, as has been discussed in relation to Fig. 5*a*, saturation due to recombination of *F* centres occurs. At saturation, the maximum value of χ_{min} is found to be 75%. That this is similar for both damaging agents again indicates there is little contribution from direct nuclear recoil processes.

It would obviously be of considerable interest to investigate whether the relatively low nuclear contribution to damage reported here for ^{16}O ions is present also for even heavier ions, and at what masses the effects of atomic displacement become significant.

Acknowledgments

The scattering chamber and contents described in this paper were wholly constructed by the technical staff of this School, to whom thanks are due. The ^{16}O induced damage described in Section 5*a* was studied in collaboration with Mr J. Söderbaum, to whom we are indebted for the depth analysis. We gratefully acknowledge assistance from Dr P. B. Treacy with data collection and in valuable discussions of the results.

References

Anderson, J. U., Davies, J. A., Nielson, K. O., and Andersen, S. L. (1965). *Nucl. Instrum. Methods* **38**, 210.
Carriveau, G. W. (1970). *J. Phys.* E **3**, 929.
Hobbs, L. W., Hughes, A. E., and Pooley, D. (1972). *Phys. Rev. Lett.* **28**, 234.
Hobbs, L. W., Hughes, A. E., and Pooley, D. (1973). *Proc. R. Soc. London* A **332**, 167.
Hollis, M. J. (1972). *Nucl. Instrum. Methods* **104**, 1.
Hollis, M. J., Newton, C. S., and Price, P. B. (1973). *Phys. Lett.* A **44**, 243.
Ivey, H. (1947). *Phys. Rev.* **72**, 341.
Lindhard, J. (1965). *Mat. Fys. Medd. Dan. Vid. Selsk.* **34**, No. 14.
Lindhard, J., Scharff, M., and Schiøtt, H. E. (1963). *Mat. Fys. Medd. Dan. Vid. Selsk.* **33**, No. 14.
Newton, C. S., Alexander, R. B., Clark, G. J., Hay, H. J., and Treacy, P. B. (1976). *Nucl. Instrum. Methods* **132**, 213.
Northcliffe, L. C., and Schilling, R. F. (1970). *Nucl. Data Tables* **7**, 233.
Pooley, D. (1966*a*). *Proc. Phys. Soc. London* **87**, 245, 257.
Pooley, D. (1966*b*). *Brit. J. Appl. Phys.* **17**, 855.
Price, P. B., Hollis, M. J., and Newton, C. S. (1973). *Nucl. Instrum. Methods* **108**, 605.
Woldseth, R. (1973). 'X-ray Energy Spectrometry', p. **2**.6 (Kevex: California).

Manuscript received 10 September 1979, accepted 30 January 1980